D. Amitrano, G. Di Martino, A. Iodice, D. Riccio, G. Ruello “Small Reservoirs Extraction in Semiarid Regions Using Multitemporal Synthetic Aperture Radar Images”, *IEEE J. Sel. Topics Appl. Earth Observ.*, vol. 10, no. 8, pp. 3482-3492, Aug. 2017. DOI: 10.1109/JSTARS.2017.2692959.

Small Reservoirs Extraction in Semiarid Regions Using Multitemporal Synthetic Aperture Radar Images

Donato Amitrano, *Member, IEEE*, Gerardo Di Martino, *Member, IEEE*, Antonio Iodice, *Senior Member, IEEE*, Daniele Riccio, *Fellow, IEEE*, and Giuseppe Ruello, *Member, IEEE*

***Abstract*—In this paper, we introduce a novel framework for small reservoirs extraction in semiarid environment. The task is accomplished through the introduction of a pseudoprobability index derived from multitemporal synthetic aperture radar RGB images. These products are characterized by the ease of interpretation for nonexpert users, and the possibility to be processed using simple algorithms, allowing, in this case, for the definition of an ad hoc band ratio for feature extraction. The reliability of the proposed approach is demonstrated through a case study in Burkina Faso in which 19 reservoirs up to about 6000 m^2 extent were tested. The obtained accuracy with respect to the available ground truth is higher than 88%.**

***Index Terms*—Change detection, level-1α products, multitemporal, semiarid environment, small reservoirs, synthetic aperture radar (SAR), water resource management.**

I. Introduction

INFORMATION about the extent of water surfaces is fundamental for water resource monitoring [1]–[3]. In fact, fresh water is crucial for terrestrial life, providing a unique resource for various human activities and several ecosystem services, guaranteeing high levels of biodiversity [4]. However, our knowledge of river networks and inland water storage is rather scarce [5]. In this context, recent advances in remote sensing allow for a better understanding of water dynamics, thus introducing significant improvements, as an example, in the mapping of floods [6]–[10] and prediction of droughts [11].

Dealing with inland water, several methods were developed in the past remote sensing literature to delineate water bodies and enhance their presence. As stated in [12], these methods generally make use of reflected solar radiation or active microwave systems.

Solar radiation-based methods can be classified in single-band and multiband methods [12]. In the first case, near-infrared radiation (NIR) is used, because it is strongly absorbed by water and highly reflected by vegetation and terrain. Thresholding is then applied to isolate the water class. However, moist and bare soils could exhibit low reflectance at NIR frequencies. Therefore, the joint use of NIR and visible frequencies has been proposed to enhance the presence of surface water with respect to terrestrial features, thus leading to the formulation of the normalized difference water index (NDWI) [12] and its modifications [13].

Multispectral sensors allows for the definition of spectral indices, whose amplitude is related to some physical characteristic of the feature of interest. As an example, the NDWI is related to the water turbidity [12]. This index provides an easily comprehensible information for nonexpert remote sensing users. Therefore, it is often exploited in applications [14]–[18].

Main limitations of this approach are: 1) The low resolution of the most used sensors (Landsat, Meris) which is a significant constraint in the monitoring of small reservoirs with few thousand square meters of extension, and 2) the cloud coverage. During either winter, in temperate areas, or the rainy season, in tropical environment, the extremely probable cloud coverage hampers the use of optical sensors.

The use of active microwave systems, in particular synthetic aperture radar (SAR), can help to overcome the above-described hurdles. In fact, these sensors are very attractive for water resources management applications thanks to their high resolution, short revisit time, and independence from weather conditions. Using SAR images, water body detection is mainly addressed as an image segmentation problem. Amitrano *et al.* [2] suggested to extract small reservoirs in semiarid Burkina Faso using a simple threshold on the amplitude images. Similar, thresholding-based approaches were proposed in [19] and [3]. Gaetano *et al.* [20] proposed a more general interactive segmentation framework exploiting Markov random fields. Boni *et al.* [8] proposed an integrated system for flood monitoring based on the joint exploitation of satellite acquisitions and flood forecasts. Martinis *et al.* compared four operational water and flood detection approaches developed at DLR, i.e., the water mask processor, the rapid mapping of flooding, the TSX flood service, and the TanDEM-X water indication mask processor [21]. Garcia-Pintado *et al.* [22] proposed a flood forecasting system supported by satellite SAR acquisitions. D'Addabbo *et al.* [23] introduced a Bayesian network to integrate multitemporal SAR data with geomorphic and other ground information for flood detection. The same topic was faced in [10], where the use of

Manuscript received November 21, 2016; revised February 17, 2017; accepted April 4, 2017. *(Corresponding author: Donato Amitrano.)*

The authors are with the Department of Electrical Engineering and Information Technology, University of Napoli Federico II, Napoli 80138, Italy (e-mail: donato.amitrano@unina.it; gerardo.dimartino@unina.it; iodice@unina.it; dariccio@unina.it; ruello@unina.it).

Color versions of one or more of the figures in this paper are available online at http://ieeexplore.ieee.org.

Digital Object Identifier 10.1109/JSTARS.2017.2692959

both supervised and unsupervised methods, and of multimodal data is investigated. Anyway, identification of water surfaces is still an open challenge, as witnessed by the high number of valuable contributions dealing with this problem.

In this paper, we address the problem of small reservoirs extraction exploiting change detection applied on multitemporal Level-1α RGB products [24]. They are bitemporal images combining a reference acquisition with a test one, whose principal characteristics are the interpretability (thanks to an opportune, end-user-oriented color-coding of the SAR information), and the possibility to be processed with simple algorithms for information extraction [25], [26]. In particular, they allow for the introduction of indices to enhance the presence of a certain image feature [27]. Here, we present a temporary water index suitable to be applied in semiarid environment for extracting small reservoir contours. This introduces a significant novelty with respect to the past literature. In fact, several valuable change-detection-based methods have been proposed in the past literature [28]–[30], but no water index derived from SAR data has been formulated yet. This way, computational complexity and SAR expertise are moved in the product formation phase, thus simplifying the feature extraction step. In fact, just one parameter has to be adjusted, that is the threshold to be applied to the index map.

The proposed solution can be effectively used for water resource monitoring in semiarid environments. Multispectral data have been widely employed for this task with the limitation due to cloud cover, especially during the rainy season [31]–[33]. SAR data have been used to overcome this problem [34], [35], but mainly exploiting low-resolution data. In the context of semiarid regions, small reservoirs are defined as basins with surface area smaller than 100 hectares [34]. This extension is almost at the limit of the imaging capability of a sensor like ASAR, which is one of the most exploited in the past literature. The introduction of high-resolution sensors, such as COSMO-SkyMed, allowed us to lower the dimension of the observable basins drastically, bringing it to few thousand square meters.

The paper is organized as follows. In Section II, the case study is presented, and the proposed water index is defined. The study area is located in semiarid Burkina Faso, and the objective is to extract small reservoirs exploiting the water index applied on Level-1α images derived from stripmap, 3-m resolution COSMO-SKyMed data. Experimental results and their assessment are discussed in Section III. Conclusions are drawn at the end of this paper.

II. Materials and Methods

The case study has been implemented in semiarid Burkina Faso (Western Africa). The study area is located in the Yatenga region, in the North of the country. It is approximately 40×40 km^2 wide. The dataset we exploited for the study is composed by a series of COSMO-SkyMed stripmap acquisitions with 3-m spatial resolution (see Table I for a summary of the images used in this study).

Burkina Faso, as well as the whole Sahel, is characterized by a particularly vulnerable environment due to the scarce rainfalls. Therefore the growth of vegetation is possible only during a limited period of the year, making terrains very prone to erosion phenomena. The combination of water scarcity and soil erosion has a serious impact on terrain productivity and on the available food provisions [36] in countries where the demographic pressure is among the highest in the world.

TABLE I
Summary of the Data Used in this Study

Acquisition date	Sensor	Resolution	Polarization	Mode
28/4/2011	CSK	3×3 (m)	HH	Stripmap
15/8/2010	CSK	3×3 (m)	HH	Stripmap
31/8/2010	CSK	3×3 (m)	HH	Stripmap

Images are combined in two Level-1α products sharing the reference band, i.e., the 28/4/2011 acquisition.

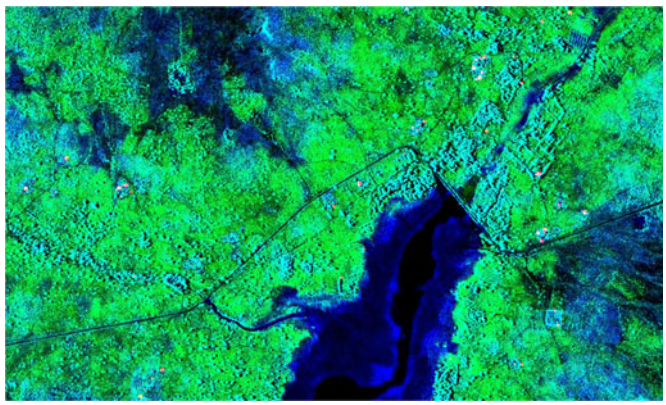

Fig. 1. Level-1α product, particular of a dam in a rural area of Burkina Faso. Blue band: April 28, 2011 (dry season, reference image); green band: August 31, 2010 (wet season, test image, i.e., the acquisition in which changes are evaluated).

The international community is well aware of these problems and many initiatives for their monitoring, prevention, and mitigation have been promoted. In particular, the TIGER initiative launched by the European Space Agency [37] represents the most relevant program of the last decade concerning water resource management supported by remotely sensed (mainly optical) data.

Using SAR data, the presence of temporary surface water can be detected through change detection by comparing the electromagnetic (EM) response of a reference image with that of a test one [24]. In a semiarid environment, a suitable reference is an image acquired during the dry season, when the landscape is almost completely dry [24]. Here, the change detection is implemented exploiting multitemporal images combined in a Level-1α RGB composite. This class of products is obtained through multitemporal processing of several SLC images acquired over the same scene, and combined in such way to favor the recognition of some scene features (in this case water and vegetation) through a suitable color rendering of the information (the interested reader can find further details about these products in [24]).

An example of such products is provided in Fig. 1. The blue band represents the amplitude of the reference image. It has been acquired on April 2011, at the peak of the dry season [38]. The

green band (test image) represents the amplitude of the image in which changes are evaluated. It has been acquired on August 2010, during the wet season. The red band is reserved to the interferometric coherence between the two images (it is useful for identifying small settlements).

This combination allows for displaying in natural colors the most important features of the study area. In fact, surface water is rendered in blue. This is due to the dominance of the EM scattering from the terrain in the basin area during the dry season (blue band) with respect to the EM scattering from surface water in the wet season (green band). Vegetation is displayed in green, due to the volumetric backscattering contribution triggered by its growing during the wet season. For further information about Level-1α processing, the reader can refer to [24].

The above-mentioned considerations lead us to define a seasonal water presence pseudoprobability as follows:

$$\text{SWPP} = \hat{G}^2 \left(\frac{B-G}{B+G} \right), \quad \text{SWPP} \in [-1, 1] \tag{1}$$

in which SWPP is the acronym for seasonal water pseudoprobability and $\hat{G}$ is given by

$$\hat{G} = \left(1 - \frac{G}{255} \right). \tag{2}$$

In (1), the first factor at the right-hand side enhances the value of SWPP for those pixels lacking the green band contribution. They are likely to represent seasonal surface water. Moreover, it is useful to drop the SWPP response from eroded terrains, whose return is typically slightly higher than that of surface water, and stable throughout the year [39].

The second factor at right-hand side attenuates the SWPP value for pixels whose green and blue response is comparable. Pixels having a dominant response in the green band (vegetation) assume negative values of the SWPP. Pixels for which the blue band is dominant assume positive SWPP values. Therefore, the threshold identifying surface water has to be searched for into the interval $]0, 1]$.

The SWPP formulation does not include the interferometric coherence. In fact, this quantity is expected to be negligible on objects unstable with respect to phase such as water surfaces.

Physically, the SWPP is related to the state of terrains during the acquisition of the reference scene. In fact, the higher the terrain response during this acquisition, the higher the value of the SWPP. As an example, consider the dam depicted in Fig. 1. The reader should note that around the permanent water surface (displayed in black) there is a "crown" in which the blue color is purer with respect to the rest of the basin area. This is due to the presence of vegetation at the basin's boundary during the dry season image acquisition. In this area, the SWPP will be slightly higher with respect to surrounding regions.

III. Experimental Results

The result of the application of (1) to some reservoirs of the study area is depicted in Fig. 2. In particular, in the first column of the picture, we reported the subsets of the Level-1α product concerning the considered reservoir. In this case, the test image has been acquired on August 31, 2010. In the second column, the reservoir contour has been manually extracted from the intensity (test) image. In the third column the SWPP map of the area (which covers in all cases approximately 1.5 km^2) is shown. Finally, in the fourth column, a binary mask obtained after thresholding of the SWPP map is depicted. Mathematical morphology has been applied in order to make the final mask more homogeneous and remove islands [40].

Qualitatively, the obtained results show a good agreement with the manually extracted ground truth. The threshold (set to 0.3) has been determined through visual inspection of the obtained SWPP map and a trial-and-error approach. This value should be scene adapted but not time-dependent, since it mainly depends on the state of terrains during the acquisition of the reference image.

A quantitative assessment of the proposed approach is now in order. A standard ground truth is not available. Therefore, we built it from data, exploiting our *a priori* knowledge of the study area [2], [38], [41]. We identified and extracted by visual inspection of the 31 August acquisition the contour of 19 reservoirs. This operation is of course time-consuming [42] and not trivial, due to the strong unbalance between the classes water and nonwater (reservoirs constitute about 0.01% of the whole scene), and the presence of vegetation/mud at reservoir boundary, making it difficult to recognize the contour. However, in many cases, the expert photo interpreter is able to perform reliable feature extraction [43], [44]. Therefore, we are quite confident that the retrieved contours are well representative of the real basin extension.

The reservoirs included in the ground truth have dimension between approximately 6000 and 300 000 m^2 (in general, we did not consider objects with surface area smaller than 6000 m^2). These reservoirs have been marked with a red dot in Fig. 3, in which we report the Level-1α product of the whole study area (reference image: April 28, 2011, test image: August 31, 2010). The numeric ID accompanying the red dots refers to the graph depicted in Fig. 6. The second RGB image used for the assessment has as test image the acquisition of August 15, 2010.

At first, an object-based assessment is proposed. In Fig. 3, we also emphasize possible ambiguities, defined as structures with an high SWPP (i.e., above the selected threshold) in only one or both acquisitions, but not associable to reservoirs by visual inspection. In particular, yellow dots have high SWPP on August 15. Magenta dots have high SWPP on August 31. White dots have high SWPP in both acquisitions. On August 15, we counted 13 of such structures; on August 31, the count was 17. The number of structures which persist in both dates is 6.

The first result we obtained is that all the 19 basins constituting the ground truth were detected on both 15 and 31 August images.

False alarms can be due to climatic conditions and the severe rainfalls occurring during the wet season. In fact, after a heavy rainfall, it is highly probable that the terrain shape, in some area, favors the accumulation of water in natural hollows. This makes very difficult to establish whether a detected structure is a false alarm or a tank. Therefore, we define as a false alarm a structure that is not stable on a short time scale. In fact, due to high evapotranspirations (and infiltrations), a water accumulation in a natural hollow should disappear in few days.

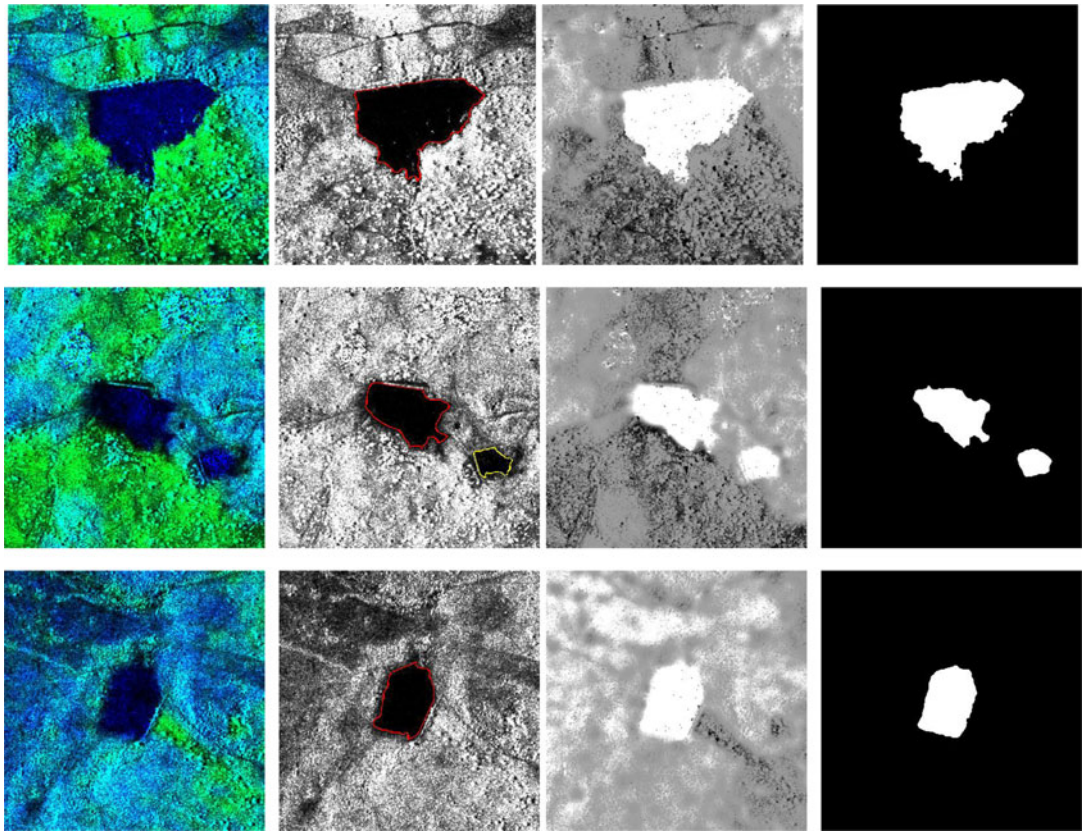

Fig. 2. Results of the application of the SWPP definition to the August 31, 2010 scene for four small reservoirs. First column: Level-1α products (reference image: April 28, 2011); second column: manually extracted water surface mask superimposed to the temporal-filtered SAR product; third column: SWPP map; fourth column: binary mask obtained thresholding the SWPP map at 0.3. Original patch dimensions: 512×512 pixels (approximately 1.5×1.5 m^2).

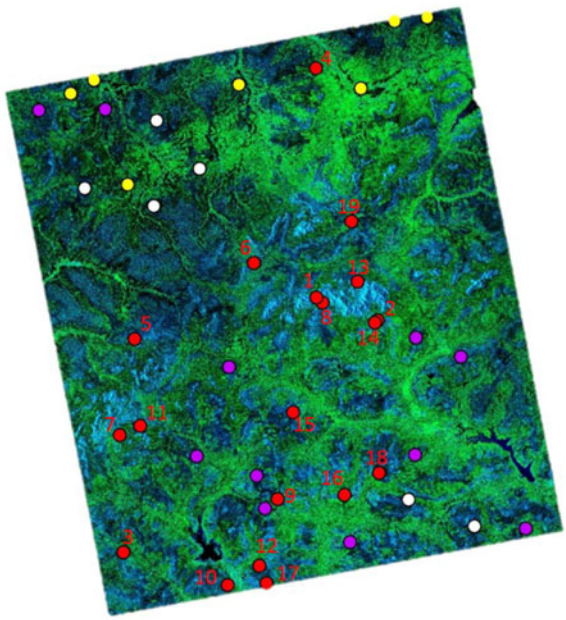

Fig. 3. Level-1α product of the study area. Reference image (blue band): April 28, 2011. Test image (green band): August 31, 2010. Red dots identify the basins assumed as ground truth, indexed with an ID referring to the graph of Fig. 6. Magenta dots indicate objects not recognized as basins by visual inspection in the image acquired on August 31, 2010. Yellow dots indicate objects not recognized as basins by visual inspection in the image acquired on August 15, 2010. White dots indicate objects not recognized as basins by visual inspection in both the aforementioned images.

The analysis of false alarms is supported by the rainfalls diagram in the study area for the years 2010 and 2011, reported in Fig. 4 [38]. In this graph, each of the indicated dates refers to an available SAR acquisition, which can be exploited to map reservoirs' state using always the same reference scene. It arises that the acquisition of August 31 is immediately preceded by a severe rainfall event. Therefore, we can argue that the higher false alarm rate should be due to this event. If we consider the acquisition of August 15, we can see that the closest rainfall occurred a couple of days before. Therefore, we can argue that the evapotranspiration phenomenon causes the reduction in the number of unidentifiable structures. As a general comment, the more intense the rainfalls in the days preceding the acquisition, the higher the probability to detect such structures. However, if two acquisitions are considered, the probability to detect objects not relevant from an hydrological viewpoint is significantly reduced. In particular, as aforementioned, by considering the acquisitions of August 15 and 31, 2010, we found 6 structures that can be assumed as false alarms.

However, in order to remark the complexity of false alarm evaluation, consider the situation depicted in Fig. 5. This picture represents a particular agricultural structure, typical of semiarid environments, constituted by terracing built in counterslope using rudimental walls for collecting rain water [45]. One of these structures as seen on a Google Earth view is shown in Fig. 5(a). This image has been acquired during the dry season on March 2013; no wet season image of the area is available.

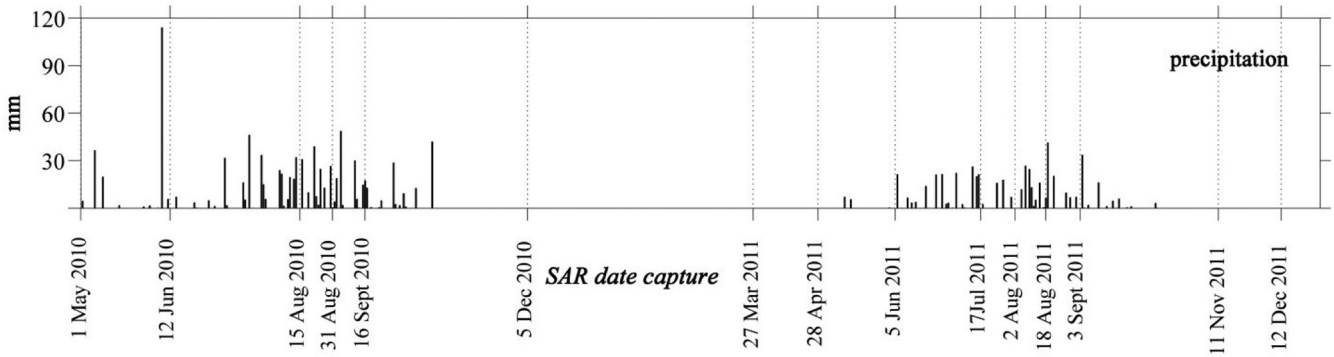

Fig. 4. Rainfalls diagram for the study area in the years 2010 and 2011.

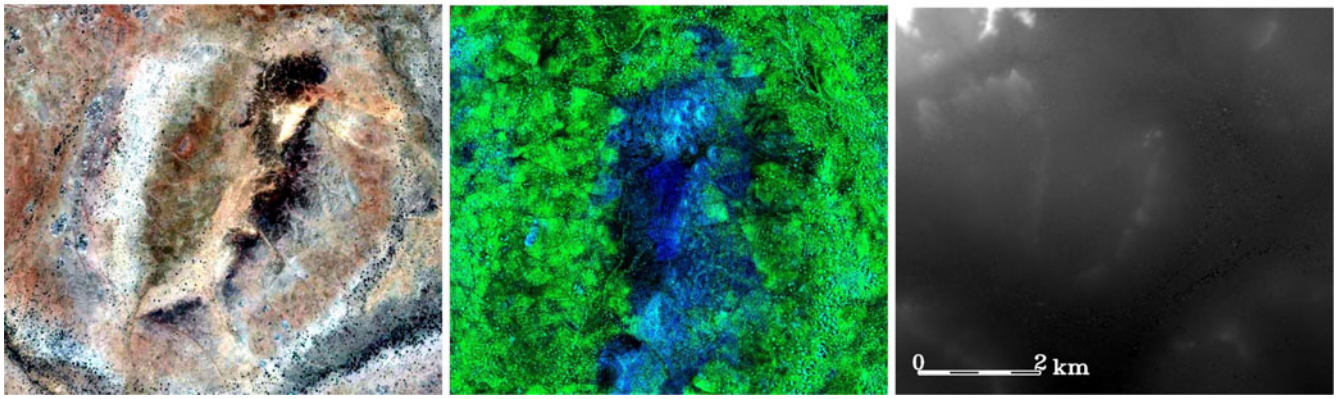

Fig. 5. Terracing built on natural hollow walls as represented in (a) Google Earth (dry season, no wet season image available), (b) Level-1α imagery (wet season), and (c) on a DEM.

This structure is one of the 6 objects we classified as false alarms (see white dots in Fig. 3). In Fig. 5(b), the same area is shown as it appears in the Level-1α product of the August 31, 2010. Finally, in Fig. 5(c), a 3-m resolution DEM of the area is shown. It arises that there is a natural hollow, whose walls are used for creating terracing. During the wet season, these structures can be covered by surface water, as well as the hollow on which they are built. Thus, they could be detected using the proposed methodology. The same situation occurs in at least four of the six cases we classified as false alarms.

In this context, evaluation of false alarms is a matter of definition, and it should be application-oriented. As an example, if the analyst is interested in the water balance of the study area, these structures should be classified as false alarms, since they are probably not hydrologically relevant. If the application is focused on agriculture, then terracing becomes as important as reservoirs, since they represent areas in which cultivation is possible. Therefore, the capability of the analyst is fundamental for recognizing the structures that could be interesting for his/her purposes. In this activity, Level-1α products make data interpretation easier with respect to Level-1 products, representing a valid support even for users with limited expertise in SAR issues.

Summarizing, dealing with small reservoirs extraction, as previously stated, we found 6 structures not relevant with the application. Indeed, this information is provided after interpretation, i.e., we aggregated in one object more (not connected) structures clearly belonging to the same scene feature.

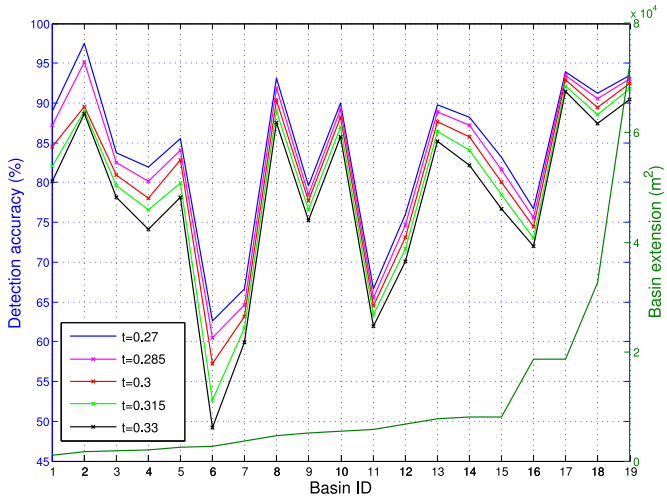

Fig. 6. Detection accuracy with respect to the extracted ground truth for the 19 analyzed reservoirs as a function of the applied threshold. Data refer to the acquisition of August 31, 2010.

A pixel-based assessment was also performed. In Fig. 6, we reported the detection accuracy with respect to the available ground truth as a function of the applied threshold (see the

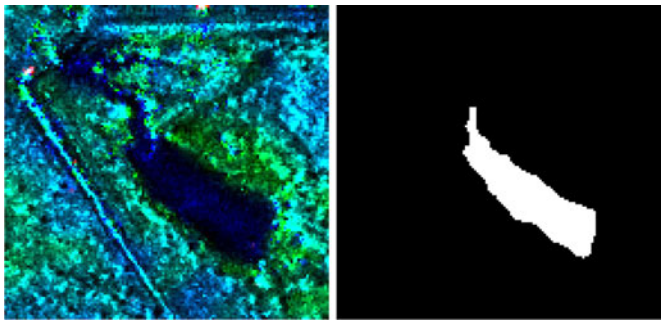

Fig. 7. Basin 7: (a) close-up of the Level-1α product and (b) its mask extracted after thresholding.

sensitivity analysis in Section III-A for details) for the 19 considered basins (see Fig. 3). Overall, the registered accuracy is of 88.8%.

As for missed detections, they are mainly related to the mixed response of boundaries in which the presence of mud and/or persistent vegetation causes the reference image scattering to be not dominant. This is the case, as an example, of the basin depicted in Fig. 7(a), which is indexed with the number 7 in Fig. 3. This basin is among those characterized by the worse performance of the detection (about 60%, see Fig. 6). In this case, the shape of the reservoir (particularly elongated and narrow in its upper part) also plays a role. In fact, the usage of mathematical morphology tends to further erode the contour, which in this case is completely lost in the upper part. The combination of the presence of mud and of the usage of mathematical morphology generally causes an underestimation of basin contours.

Operatively, the SWPP can be effectively exploited for temporal monitoring of the available water. An example is shown in Fig. 8. In particular, in the first column, we show three Level-1α products concerning the Laaba basin (ID 19 in Fig. 3). They share the reference image (acquired on April 28, 2011). The test images was acquired on March 27, 2011 (first row, dry season), August 8, 2011 (second row, wet season), and December 12, 2011 (third row, beginning of a new dry season). These representations allow for easily monitoring the state of the basin (water is displayed in blue) and of the surrounding land cover (vegetation is displayed in green).

In the second column of Fig. 8, the SWPP maps corresponding to the above-described Level-1α products are shown. Areas covered by surface water have a strong response to the SWPP and can be identified at the center of the scene. Finally, in the third column of Fig. 8, the water masks obtained via thresholding of the SWPP maps is reported. In all the cases, the threshold has been set to 0.3. In fact, as previously explained, the threshold is scene dependent but not time dependent. If the same reference image is selected, the same threshold value can be used to monitor the study area over the time. We want to remark that these binary masks have been treated just with mathematical morphology. No rejection of small regions has been implemented, in order to highlight that the SWPP thresholding restitutes almost "clean" maps, in which water surfaces are well separated from land.

As discussed in [2], basins' shoreline, combined with their bathymetric profile, can be transformed in a Level-2 product carrying the retained water volume.

A. Considerations on the Threshold and Sensitivity Analysis

The most critic operation of the proposed methodology is the thresholding to be applied to the SWPP map to retrieve the reservoirs mask. In fact, similarly to any threshold-based method, the selected value can greatly affect the quality of the retrieved feature map. A starting point to determine it can be provided by automatic thresholding algorithms, like the Otsu algorithm [46], which is one of the most popular and widely available in open-source/commercial software suites. However, this method performs at its best, when the number of pixels in each of the two scene classes is comparable [47]. Therefore, to make this algorithm exploitable, a supervised procedure inspired to the one suggested in [48] was implemented. In particular, after visual inspection of the image, some patches have been retrieved around the reservoirs. Then, the Otsu algorithm has been run for each patch to retrieve a local threshold. The global threshold, to be applied to the whole image, is assumed to be the average of the local thresholds. The value obtained using ten patches is $t = 0.3031$, that is very close to the one we determined through a trial-and-error approach (i.e., $t = 0.3$). This is due to our expertise with the scene. Conversely, a nonexpert operator can benefit from the patch-based threshold determination, which requires just the selection of some significant areas of interest.

The sensitivity analysis with respect to variations of the threshold is now in order. We assume that the "optimum" threshold is the one determined with the trial-and-error-approach, i.e., $t = 0.3$. To perform this analysis, we repeated the entire processing varying the threshold of an amount of $\pm 5\%$ and $\pm 10\%$. Therefore, the threshold values $t = 0.285$, $t = 0.315$, $t = 0.27$, and $t = 0.33$ were considered. The obtained results were compared with those obtained setting the threshold value $t = 0.3$.

In Fig. 6, we show the detection accuracy for each of the considered reservoirs as a function of the applied threshold (data refer to the 31 August acquisition). Aggregated results are presented in Table II for both 31 August and 15 August acquisitions. The parameters we used for the assessment are the overall accuracy and the false alarm rate. A pixel-based and an object-based assessment were performed. In the false alarm column, data in parentheses are those obtained after the cross comparison between the two considered dates. In fact, as explained above, false alarm rate can be reduced excluding objects not stable on a short temporal scale. Finally, concerning false alarms, all the objects not identified as reservoirs by visual inspection were counted, regardless they evidently belong to the same structure.

The outcomes of the performed experiments are the following.

1) Moving the threshold upward (even significantly) did not cause missed detection and did not affect significantly the overall accuracy.
2) When the threshold is moved downward significantly (-10%) a relevant increase of false alarms is registered.

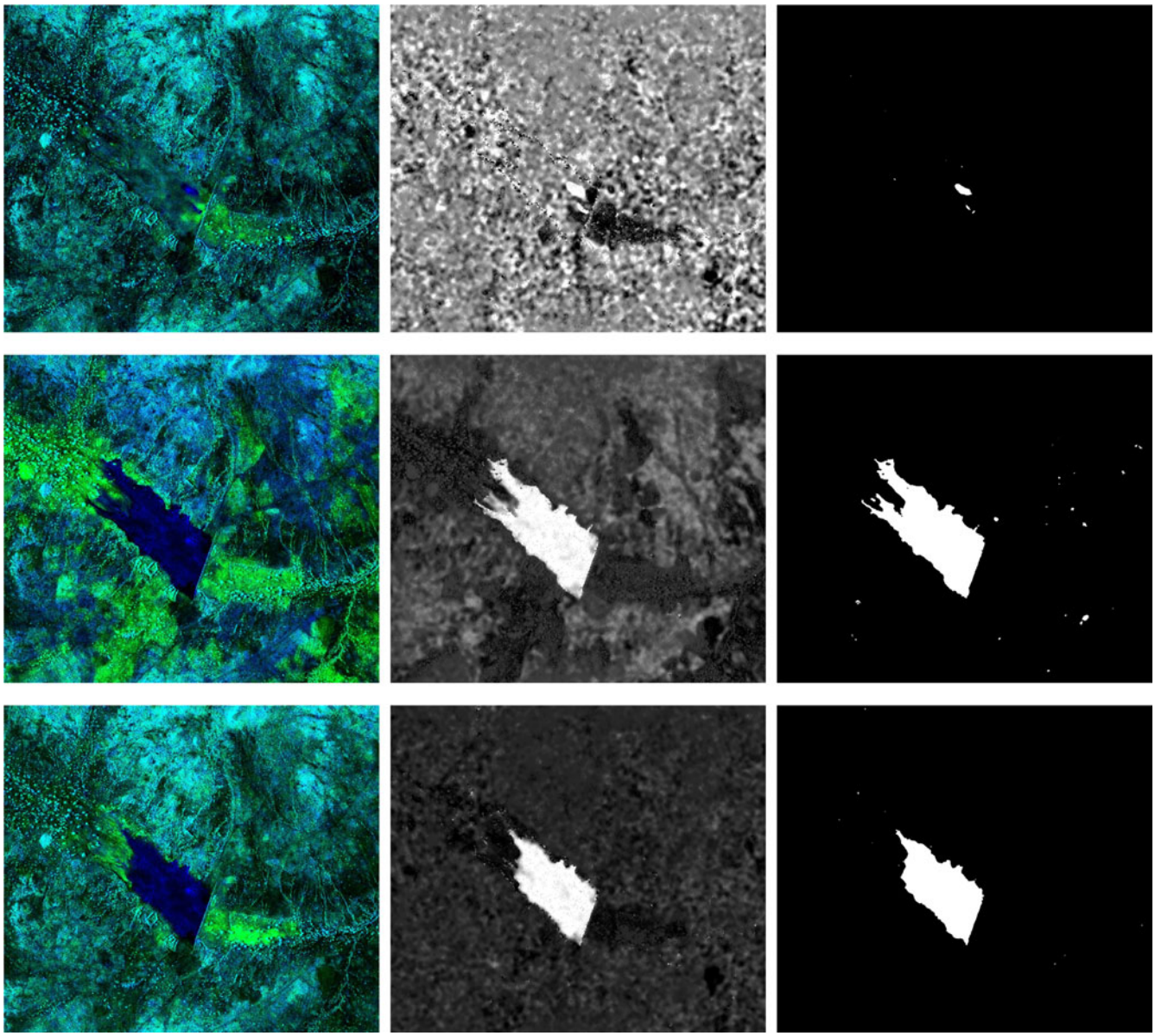

Fig. 8. Laaba basin, temporal monitoring. First column: Level-1α products (reference image April 28, 2011). Second column: SWPP maps. Third column: water masks obtained thresholding the SWPP maps at 0.3 (mathematical morphology has been applied, no rejection of small regions implemented). Test images of Level-1α products: first row—March 27, 2011 (dry season), second row—August 2, 2011 (wet season), third row—December 12, 2011 (beginning of a new dry season).

3) The false alarm rate can be significantly reduced through cross comparison of two acquisitions made with short temporal baseline.
4) The detection accuracy is rather high for all the performed experiments.

Based on these experiments, we can conclude that the proposed method is rather robust to variation of the selected threshold, especially when this value is moved upward with respect to the "optimum" value.

B. Comparison With Other Methods

The proposed methodology is composed by two steps: 1) the computation of the seasonal water pseudoprobability and 2) the determination of the best threshold. Thus, the feature extraction problem is related to the binary segmentation of the SWPP feature map. Clearly, this process can be also applied directly to SAR data. Therefore, in this section, we assess the performance of our methodology through the following experiments.

1) Comparison with fixed thresholding method and varying the input feature map. In other words, we adopt the trial-and-error approach to segment two different feature maps, i.e., the SWPP map and the band ratio map.
2) Comparison with fixed input feature map and varying the segmentation method. In this case, we fix the base map for reservoir extraction (i.e., the SWPP map) and test the trial-and-error approach with other segmentation methods.

TABLE II
SWPP RESERVOIR EXTRACTION SENSITIVITY ANALYSIS

Date	T	OA		FA	
		P (%)	O	P $\times E-4$	O
31/8	0.3	88.8	19/19	2.38 (1.06)	37 (13)
	0.27	90.5	19/19	4.31 (1.82)	80 (31)
	0.33	85.1	19/19	1.62 (0.82)	24 (11)
	0.285	89.7	19/19	3.16 (1.39)	50 (19)
	0.315	86.4	19/19	1.95 (0.90)	29 (11)
15/8	0.3	89.8	19/19	2.64 (1.32)	48 (13)
	0.27	91.1	19/19	4.73 (1.78)	97 (31)
	0.33	88.4	19/19	1.68 (0.79)	23 (11)
	0.285	89.1	19/19	1.92 (1.35)	70 (19)
	0.315	90.6	19/19	4.30 (0.87)	27 (11)

T: applied threshold, OA: overall accuracy, FA: false alarm rate. P: pixel-based assessment, O: object-based assessment. In the false alarm column, values in parenthesis are those obtained after cross comparison with the closest available acquisition.

TABLE III
FIXED THRESHOLDING

Date	Method	T	OA		FA	
			P (%)	O	P $\times E^{-4}$	O
31/8	SWPP	0.3	88.8	19/19	2.38 (1.06)	37 (13)
	BR	2.5	82.2	19/19	2.00 (0.82)	32 (11)
	BR	2.25	85.7	19/19	4.26 (1.36)	68 (19)
15/8	SWPP	0.3	89.8	19/19	2.64 (1.32)	48 (13)
	BR	2.5	87	19/19	4.13 (0.78)	61 (11)
	BR	2.25	89.5	19/19	8.54 (1.32)	94 (19)

Comparison between SWPP-based and band ratio-based (BR) reservoirs extraction with threshold determined using a trial-and-error approach. T: applied threshold, OA: overall accuracy, FA: false alarm rate. P: pixel-based assessment, O: object-based assessment. In the false alarm column, values in parenthesis are those obtained after cross comparison with the closest available acquisition.

3) Comparison of the whole methodology with direct classification of SAR images. Here, we compare our approach with simple and popular SAR segmentation methods.

1) Fixed Thresholding: We start the assessment comparing the SWPP-based feature extraction with the most similar procedure, i.e., a band ratio-based extraction (see Table III). In both cases, the trial-and-error approach for thresholding determination was adopted.

At first, we set the threshold for the ratio image to $t = 2.5$. The comparison with the SWPP-based extraction (using $t = 0.3$) shows that the overall accuracy is rather lower, and the false alarm rate slightly better. Therefore, we lowered the threshold of 10% ($t = 2.25$), in order to get the band-ratio accuracy closer to the one obtained using the SWPP, evaluating at the same time the effect on the false alarm rate. We found that the band-ratio accuracy was still lower than the SWPP accuracy, and that the false alarm rate was higher with respect to the one obtained using the SWPP. Therefore, we can conclude that in order to reach the same performance of the SWPP-based extraction, using a band ratio a significantly higher false alarm rate has to be expected.

TABLE IV
FIXED SWPP INPUT FEATURE MAP

Date	Method	T	OA		FA	
			P (%)	O	P $\times E^{-4}$	O
31/8	SWPP	0.3	88.8	19/19	2.38 (1.06)	37 (13)
	KM	6	94.9	19/19	115 (12.8)	2077 (293)
	KM	7	93.9	19/19	57.9 (4.74)	1207 (111)
	KM	8	92.2	19/19	17.4 (1.36)	392 (21)
	KM	9	89.8	19/19	5.89 (1.09)	120 (13)
15/8	SWPP	0.3	89.8	19/19	2.64 (1.32)	48 (13)
	KM	6	93.5	19/19	18.9 (13.0)	388 (293)
	KM	7	92.17	19/19	7.50 (4.84)	156 (111)
	KM	8	89.51	19/19	2.27 (1.41)	37 (21)
	KM	9	89.3	19/19	2.01 (1.10)	30 (13)

Comparison between thresholding-based and *k*-means-based (KM) reservoirs extraction. T: applied threshold or number of clusters, OA: overall accuracy, FA: false alarm rate. P: pixel-based assessment, O: object-based assessment. In the false alarm column, values in parenthesis are those obtained after cross comparison with the closest available acquisition.

2) Fixed Input Feature Map: In this section, we fix the input feature map, i.e., the proposed SWPP map, and verify the reliability of the trial-and-error approach for threshold determination comparing the obtained results with those output by other simple segmentation techniques. In particular, the *k*-means algorithm was tested due to its availability in commercial/open-source software suites and popularity in the end-user community. As shown in Table IV, several experiments have been performed varying the number k of input clusters. In this case, the final basin mask is given by the cluster with the highest SWPP mean.

We found that, using the *k*-means, the best tradeoff between overall accuracy and false alarm rate is obtained by setting $k = 9$. With this parameter setting (computational time was of some hours using an 8-core, 24-GB RAM machine), results are comparable with those obtained through trial-and-error thresholding. Further increase of the number of clusters caused an unacceptable rising of false alarms due to their aggregation in few mottled dominant classes.

3) Direct Classification of SAR Images: In this section, we test the reliability of the whole methodology with respect to feature extraction based on direct classification of SAR images. We tested *k*-means and maximum likelihood classifiers. In all cases, the same information content of a Level-1α product, i.e., a couple of SAR images, was exploited to classify.

As for the *k*-means, we ran the algorithm setting as output from 5 to 15 clusters having no convergence for all the experiments after 100 iterations and several hours processing time (increasing as the number of output clusters increases).

As for the ML classification, the adopted procedure is the following. We performed a three-class classification (water, vegetation, bare soil) selecting training sets whose extension is related to the occurrence of the class on the scene. Therefore, the biggest one was for the bare soil class. The training set for the water class was the smallest, with an extension of about 10% of the available ground truth. Results of this experiment are reported in Table V. After the classification, the class with the highest SWPP mean was selected as representative of the scene's reservoirs. We registered a significantly lower overall accuracy with

TABLE V
DIRECT CLASSIFICATION OF SAR IMAGES

Date	Method	T	OA		FA	
			P (%)	O	P $\times E^{-4}$	O
31/8	SWPP	0.3	88.8	19/19	2.38 (1.06)	37 (13)
	KM		No convergence			
	ML	na	79.39	19/19	7.63 (0.37)	134 (5)
15/8	SWPP	0.3	89.8	19/19	2.64 (1.32)	48 (13)
	KM		No convergence			
	ML	na	80.7	19/19	0.97 (0.37)	20 (5)

Comparison between SWPP-based, *k*-means-based (KM) and maximum likelihood-based (ML) feature extraction. T: applied threshold, OA: overall accuracy, FA: false alarm rate. P: pixel-based assessment, O: object-based assessment. In the false alarm column, values in parenthesis are those obtained after cross comparison with the closest available acquisition.

respect to the SWPP-based classification, as well as a slightly lower false alarm rate. The conclusion is that, provided a good knowledge of the scene, allowing for a suitable training of the classifier, the ML algorithm could be a valid alternative to solve the problem of reservoir identification, if a rather low detection rate is acceptable for the application.

IV. CONCLUSION

In this paper, we presented a novel methodology for temporary water body detection in semiarid environment. It is suitable to be applied to Level-1α RGB multitemporal SAR composites. In particular, we introduced a seasonal water pseudoprobability, whose expression is given by a simple weighted band-ratio between a reference and a test image, representing the situation in which the seasonal water coverage occurs.

The proposed method allowed for detecting all the reservoirs in the study area with limited occurrence of false alarms. This is encouraging, since in the study area, basins are not mapped and often built autonomously by local communities without a governmental coordination. Therefore, the most important information the analyst needs is about the presence or not of a water surface in a certain area.

The effectiveness of the proposed method is related to the selection of the reference band composing the input Level-1α product. In fact, the seasonality of the water is related to its absence during the acquisition of this image. Therefore, a suitable choice for the reference image is an acquisition made at the peak of the dry season, when the environment is almost completely dry.

The performance of our methodology was compared with that of several literature algorithms obtaining satisfying results. In particular, three approaches have been tested: fixed thresholding method, fixed input feature map, and direct segmentation. In all the experiments, the proposed methodology demonstrated to be a valid alternative to popular algorithms with higher complexity.

A sensitivity analysis was also performed, demonstrating that the method is rather robust with respect to variations of the "optimum" threshold value, here determined with a trial-and-error approach. A simple supervised procedure for threshold determination has been also proposed to help nonexpert user in this task.

The presented technique provides a quick solution for the detection of temporary water bodies detection. Our approach is particularly oriented toward the end-user community because it allows for operating with a simple tool, moving the complexities related to scattering mechanisms and the computational burden in the products formation phase.

ACKNOWLEDGEMENTS

The authors would like to thank the Italian Space Agency (ASI) for providing the Burkina Faso dataset under the aegis of the "HydroCIDOT" project and the anonymous reviewers for their useful suggestions.

REFERENCES

[1] P. S. Frazier and K. J. Page, "Water body detection and delineation with landsat TM data," *Photogrammetric Eng. Remote Sens.*, vol. 66, no. 12, pp. 1461–1467, 2000.
[2] D. Amitrano *et al.*, "Modeling watershed response in semiarid regions with high resolution synthetic aperture radars," *IEEE J. Sel. Topics Appl. Earth Observ.*, vol. 7, no. 7, pp. 2732–2745, Jul. 2014.
[3] S. Zhang, S. Foerster, P. Medeiros, J. Carlos de Araujo, M. Motagh, and B. Waske, "Bathymetric survey of water reservoirs in north-eastern Brazil based on TanDEM-X satellite data," *Sci. Total Environ.*, vol. 571, pp. 575–593, 2016.
[4] S. C. J. Palmer, T. Kutser, and P. D. Hunter, "Remote sensing of inland waters: Challenges, progress and future directions," *Remote Sens. Environ.*, vol. 157, pp. 1–8, 2015.
[5] D. E. Alsdorf and D. P. Lettenmaier, "Tracking fresh water from space," *Science*, vol. 301, pp. 1491–1494, 2003.
[6] J. Martinez and T. Le Toan, "Mapping of flood dynamics and spatial distribution of vegetation in the Amazon floodplain using multitemporal SAR data," *Remote Sens. Environ.*, vol. 108, no. 3, pp. 209–223, 2007.
[7] K. Voormansik, J. Praks, O. Antropov, J. Jagomgi, and K. Zalite, "Flood mapping with TerraSAR-X in forested regions in Estonia," *IEEE J. Sel. Topics Appl. Earth Observ.*, vol. 7, no. 2, pp. 562–577, Feb. 2014.
[8] G. Boni *et al.*, "A prototype system for flood monitoring based on flood forecast combined with COSMO-SkyMed and Sentinel-1 data," *IEEE J. Sel. Topics Appl. Earth Observ.*, vol. 9, no. 6, pp. 2794–2805, Jun. 2016.
[9] L. Pulvirenti, N. Pierdicca, M. Chini, and L. Guerriero, "Monitoring flood evolution in vegetated areas using COSMO-SkyMed data: The Tuscany 2009 case study," *IEEE J. Sel. Topics Appl. Earth Obs. Remote Sens.*, vol. 6, no. 4, pp. 1807–1816, Aug. 2013.
[10] N. Longbotham *et al.*, "Multi-modal change detection, application to the detection of flooded areas: Outcome of the 2009 data fusion contest," *IEEE J. Sel. Topics Appl. Earth Observ.*, vol. 5, no. 1, pp. 331–342, Feb. 2012.
[11] A. AghaKouchak *et al.*, "Remote sensing of drought: Progress, challenges and opportunities," *Rev. Geophys.*, vol. 53, no. 2, pp. 452–480, 2015.
[12] S. K. McFeeters, "The use of the Normalized Difference Water Index (NDWI) in the delineation of open water features," *Int. J. Remote Sens.*, vol. 17, no. 7, pp. 1425–1432, 1996.
[13] H. Xu, "Modification of normalised difference water index (NDWI) to enhance open water features in remotely sensed imagery," *Int. J. Remote Sens.*, vol. 27, no. 14, pp. 3025–3033, 2006.
[14] D. A. Roshier, P. H. Whetton, R. J. Allan, and A. I. Robertson, "Distribution and persistence of temporary wetland habitats in arid Australia in relation to climate," *Austral Ecol.*, vol. 26, no. 4, pp. 371–384, 2001.
[15] A. Davranche, G. Lefebvre, and B. Poulin, "Wetland monitoring using classification trees and spot-5 seasonal time series," *Remote Sen. Environ.*, vol. 114, no. 3, pp. 552–562, 2010.
[16] T. Sakamoto, N. V. Nguyen, A. Kotera, H. Ohno, N. Ishitsuka, and M. Yokozawa, "Detecting temporal changes in the extent of annual flooding within the cambodia and the vietnamese mekong delta from MODIS time-series imagery," *Remote Sens. Environ.*, vol. 109, no. 3, pp. 295–313, 2007.

[17] S. K. McFeeters, "Using the Normalized Difference Water Index (NDWI) within a geographic information system to detect swimming pools for mosquito abatement: A practical approach," *Remote Sens.*, vol. 5, no. 7, pp. 3544–3561, 2013.
[18] J. C. Campos, N. Sillero, and J. C. Brito, "Normalized difference water indexes have dissimilar performances in detecting seasonal and permanent water in the Sahara-Sahel transition zone," *J. Hydrol.*, vol. 464-465, pp. 438–446, 2012.
[19] I. Heine, T. Francke, C. Rogass, P. H. A. Medeiros, A. Bronstert, and S. Foerster, "Monitoring seasonal changes in the water surface areas of reservoirs using terraSAR-X time series data in semiarid northeastern Brazil," *IEEE J. Sel. Topics Appl. Earth Observ.*, vol. 7, no. 8, pp. 3190–3199, Aug. 2014.
[20] R. Gaetano *et al.*, "Exploration of multitemporal COSMO-SkyMed data via tree-structured MRF segmentation," *IEEE J. Sel. Topics Appl. Earth Observ.*, vol. 7, no. 7, pp. 2763–2775, Jul. 2014.
[21] S. Martinis *et al.*, "Comparing four operational SAR-based water and flood detection approaches," *Int. J. Remote Sens.*, vol. 36, no. 13, pp. 3519–3543, 2015.
[22] J. Garcia-Pintado *et al.*, "Satellite-supported flood forecasting in river networks: A real case study," *J. Hydrol.*, vol. 523, pp. 706–724, 2015.
[23] A. D'Addabbo, A. Refice, G. Pasquariello, F. P. Lovergine, D. Capolongo, and S. Manfreda, "A Bayesian network for flood detection combining SAR imagery and ancillary data," *IEEE Trans. Geosci. Remote Sens.*, vol. 54, no. 6, pp. 3612–3625, Jun. 2016.
[24] D. Amitrano, G. Di Martino, A. Iodice, D. Riccio, and G. Ruello, "A new framework for SAR multitemporal data RGB representation: Rationale and products," *IEEE Trans. Geosci. Remote Sens.*, vol. 53, no. 1, pp. 117–133, Jan. 2015.
[25] D. Amitrano, G. Di Martino, A. Iodice, D. Riccio, and G. Ruello, "An end-user-oriented framework for the classification of multitemporal SAR images," *Int. J. Remote Sens.*, vol. 37, no. 1, pp. 248–261, 2016.
[26] D. Amitrano *et al.*, "Multitemporal level-1β products: Definitions, interpretation, and applications," *IEEE Trans. Geosci. Remote Sens.*, vol. 54, no. 11, pp. 6545–6562, Nov. 2016.
[27] D. Amitrano *et al.*, "Urban areas enhancement in multitemporal SAR RGB images using adaptive coherence window and texture information," *IEEE J. Sel. Topics Appl. Earth Observ.*, vol. 9, no. 8, pp. 3740–3752, Aug. 2016.
[28] S. G. Dellepiane and E. Angiati, "A new method for cross-normalization and multitemporal visualization of SAR images for the detection of flooded areas," *IEEE Trans. Geosci. Remote Sens.*, vol. 50, no. 7, pp. 2765–2779, Jul. 2012.
[29] A. Refice *et al.*, "SAR and InSAR for flood monitoring: Examples with COSMO-SkyMed data," *IEEE J. Sel. Topics Appl. Earth Observ.*, vol. 7, no. 7, pp. 2711–2722, Jul. 2014.
[30] L. Pulvirenti, M. Chini, N. Pierdicca, and G. Boni, "Use of SAR data for detecting floodwater in urban and agricultural areas: The role of the interferometric coherence," *IEEE Trans. Geosci. Remote Sens.*, vol. 54, no. 3, pp. 1532–1544, Mar. 2016.
[31] J. Liebe, N. van de Giesen, and M. Andreini, "Estimation of small reservoir storage capacities in semi-arid environment: A case study in the upper east region of Ghana," *Phys. Chem. Earth. Pt. A/B/C*, vol. 30, pp. 448–454, 2005.
[32] T. Sawunyama, A. Senzanje, and A. Mhizha, "Estimation of small reservoir storage capacities in Limpopo River Basin using geographical information systems (GIS) and remotely sensed surface areas: Case of Mzingwane catchment," *Phys. Chem. Earth Pt. A/B/C*, vol. 31, no. 1516, pp. 935–943, 2006.
[33] F. Mialhe, Y. Gunnell, and C. Mering, "Synoptic assessment of water resource variability in reservoirs by remote sensing: General approach and application to the runoff harvesting systems of south India," *Water Resource Res.*, vol. 44, no. 5, 2008.
[34] F. O. Annor, N. van de Giesen, J. Liebe, P. van de Zaag, A. Tilmant, and S. N. Odai, "Delineation of small reservoirs using radar imagery in a semi-arid environment: A case study in the upper east region of Ghana," *Phys. Chem. Earth Pt. A/B/C*, vol. 34, nos. 4/5, pp. 309–315, 2009.
[35] J. Liebe, N. van de Giesen, M. Andreini, T. Steenhuis, and M. Walter, "Suitability and limitations of ENVISAT ASAR for monitoring small reservoirs in a semiarid area," *IEEE Trans. Geosci. Remote Sens.*, vol. 47, no. 5, pp. 1536–1547, May 2009.
[36] M. W. Rosengrant, C. Ringler, and T. Zhu, "Water for agriculture: Maintaining food security under growing scarcity," *Annu. Rev. Environ. Resources*, vol. 34, pp. 205–222, 2009.
[37] European Space Agency, "The TIGER initiative 2009-2012 report," European Space Agency, Paris, France, Tech. Rep., 2012.
[38] D. Amitrano *et al.*, "Effectiveness of high-resolution SAR for water resource management in low-income semi-arid countries," *Int. J. Remote Sens.*, vol. 35, no. 1, pp. 70–88, 2014.
[39] D. Amitrano *et al.*, "High resolution SAR for the monitoring of reservoirs sedimentation and soil erosion in semi arid regions," in *Proc. IEEE Int. Geosci. Remote Sens. Symp.*, 2013, pp. 911–914.
[40] P. Soille and M. Pesaresi, "Advances in mathematical morphology applied to geoscience and remote sensing," *IEEE Trans. Geosci. Remote Sens.*, vol. 40, no. 9, pp. 2042–2055, Sep. 2002.
[41] D. Amitrano *et al.*, "Sentinel-1 for Monitoring Reservoirs: A Performance Analysis," *Remote Sens.*, vol. 6, pp. 10676–10693, 2014.
[42] P. Matgen, G. Schumann, J. B. Henry, L. Hoffmann, and L. Pfister, "Integration of SAR derived river inundation areas, high precision topographic data and a river flow model toward near real-time flood management," *Int. J. Appl. Earth Observ. Geoinf.*, vol. 9, no. 3, pp. 247–263, 2007.
[43] J. B. Campbell and R. H. Wynne, *Introduction to Remote Sensing*. New York, NY, USA: Guilford Press, 2011.
[44] J. Sanjal and X. X. Lu, "Application of remote sensing in flood management with special reference to Monsoon Asia: A Review," *Natural Hazards*, vol. 33, pp. 283–301, 2003.
[45] International Institute of Rural Reconstruction, "Conservation agriculture: A manual for farmers and extension workers in Africa," International Institute of Rural Reconstruction, Nairobi, Kenya, Tech. Rep., 2005.
[46] N. Otsu, "A threshold section method from gray-level histograms," *IEEE Trans. Syst., Man, Cybern.*, vol. SMC-9, no. 1, pp. 62–66, Jan. 1979.
[47] M. Sezgin and B. Sankur, "Survey over image thresholding techniques and quantitative performance evaluation," *J. Electron. Imag.*, vol. 1, no. 13, pp. 146–168, 2004.
[48] F. Bovolo and L. Bruzzone, "A Split-based approach to unsupervised change detection in large-size multitemporal images: Application to Tsunami damage assessment," *IEEE Trans. Geosci. Remote Sens.*, vol. 45, no. 6, pp. 1658–1670, Jun. 2007.

Donato Amitrano (S'15–M'17) was born in Naples, Italy, on December 27, 1985. He received the Bachelor's degree in aerospace engineering, the Master's degree in aerospace and astronautical engineering, and the Ph.D. degree in electronic and telecommunication engineering from the University of Naples Federico II, Napoli, Italy, in 2009, 2012, and 2016, respectively.

His research interests include multitemporal SAR, remote-sensing techniques for developing countries, machine learning, human vision, SAR images interpretation and understanding, and data fusion.

Dr. Amitrano is an Invited Reviewer of some remote-sensing specialized journals such as IEEE TRANSACTIONS ON GEOSCIENCE AND REMOTE SENSING, IEEE GEOSCIENCE AND REMOTE SENSING LETTERS, *Remote Sensing*, *International Journal of Remote Sensing*, and *Remote Sensing Letters*.

Gerardo Di Martino (S'06–M'09) was born in Naples, Italy, on June 22, 1979. He received the Laurea degree (cum laude) in telecommunication engineering and the Ph.D. degree in electronic and telecommunication engineering from the University Federico II, Naples, Italy, in 2005 and 2009, respectively.

In 2009–2016, he received several research grants from the University of Naples Federico II, regarding applied electromagnetics and remote sensing topics. In 2014–2016, he also received research grants and contracts from the Italian National Consortium for Telecommunications and the Regional Center Information Communication Technology. He is currently an Assistant Professor of electromagnetics in the Department of Electrical Engineering and Information Technology, University of Naples Federico II. His research interests include microwave remote sensing and electromagnetics, with focus on electromagnetic scattering from natural surfaces and urban areas, SAR signal processing and simulation, information retrieval from SAR data, and remote sensing techniques for developing countries.

Antonio Iodice (S'97–M'00–SM'04) was born in Naples, Italy, in 1968. He received the Laurea degree (cum laude) in electronic engineering and the Ph.D. degree in electronic engineering and computer science from the University of Naples "Federico II," Naples, Italy, in 1993 and 1999, respectively.

In 1995, he was in the Research Institute for Electromagnetism and Electronic Components of the Italian National Council of Research (IRECE-CNR), Naples, Italy, and from 1999 to 2000 in Telespazio S.p.A., Rome, Italy. From 2000 to 2004 he was a Research Scientist in the Department of Electronic and Telecommunication Engineering, University of Naples "Federico II." Since 2005, he has been a Professor of electromagnetics in the Department of Electrical Engineering and Information Technology, University of Naples "Federico II." He is a Principal Investigator or Coinvestigator in several projects funded by European Union, Italian Space Agency, Italian Ministry of Education and Research, Campania Regional Government, and private companies. His research interests include microwave remote sensing and electromagnetics: modeling of electromagnetic scattering from natural surfaces and urban areas, simulation and processing of synthetic aperture radar signals, and electromagnetic propagation in urban areas.

Prof. Iodice is the author or coauthor of more than 300 papers, of which more than 80 are published on refereed journals, and the others on proceedings of international and national conferences. He received the 2009 Sergei A. Schelkunoff Transactions Prize Paper Award from the IEEE Antennas and Propagation Society, for the best paper published in 2008 on the IEEE TRANSACTIONS ON ANTENNAS AND PROPAGATION. He was recognized by the IEEE Geoscience and Remote Sensing Society as the 2015 Best Reviewer of the IEEE TRANSACTIONS ON GEOSCIENCE AND REMOTE SENSING. He is the Chair of the IEEE South Italy Geoscience and Remote Sensing Chapter.

Daniele Riccio (M'91–SM'99–F'14) was born in Naples, Italy. He received the Laurea degree (cum laude) in electronic engineering from the University of Naples Federico II, Naples, Italy, in 1989.

He is currently a Full Professor of electromagnetic theory and remote sensing in the Department of Electrical Engineering and Information Technology, University of Naples Federico II, where he is the Coordinator of the Ph.D. School in Information Technology and Electrical Engineering. He was a Research Scientist in the Italian National Research Council, Institute for Research on Electromagnetics and Electronic Components (1989–1994), a Guest Scientist in the German Aerospace Centre (DLR), Munich, Germany (1994 and 1995), a Lecturer to the Ph.D. program at the Universitat Politecnica de Catalunya, Barcelona, Spain (2006), and at the Czech Technical University, Prague, Czech Republic (2012). He is currently also a member of the Cassini Radar Science Team, Principal Investigator for international research projects on exploitation of remote sensing data and design of synthetic aperture radars, and participates to technical committees of international symposia on electromagnetics and remote sensing. He has authored three books, including *Scattering, Natural Surfaces and Fractals* (2007), and more than 400 scientific papers. His research interests include microwave remote sensing, electromagnetic scattering, synthetic aperture radar with emphasis on sensor design, data simulation and information retrieval, as well as application of fractal geometry to remote sensing.

Prof. Riccio is an Associate Editor of some journals on remote sensing. He received the 2009 Sergei A. Schelkunoff Transactions Prize Paper Award for the best paper published in 2008 on the IEEE TRANSACTIONS ON ANTENNAS AND PROPAGATION.

Giuseppe Ruello (S'00–M'04) was born in Naples, Italy, on February 12, 1975. He received the Laurea degree (cum laude) in telecommunication engineering in 1999, and the Ph.D. degree in information engineering in 2003, from the University of Naples Federico II, Naples, Italy.

In 2002 and in 2004–2005, he was a Visiting Scientist in the Department of Signal Theory and Communications, Universitat Politecnica de Catalunya, Barcelona, Spain. He is currently a Research Scientist in the Department of Electrical and Information Technology Engineering, University of Naples Federico II. His research interests include SAR remote sensing, modeling of electromagnetic scattering from natural surfaces, SAR raw signal simulation, modeling of electromagnetic field propagation in urban environment, and remote sensing techniques for low-income semiarid regions.

Dr. Ruello received a grant from the University of Naples, in 2000, to be spent in the Department of Electronic and Telecommunication Engineering for research in the field of remote sensing and in 2000, he received a grant from University of Rome La Sapienza, Rome, Italy.